ACS OMEGA

Open Access

http://pubs.acs.org/journal/acsodf

Article

Electrochemical Detection of *Pseudomonas aeruginosa* Quorum Sensing Molecule (*S*)-*N*-Butyryl Homoserine Lactone Using Molecularly Imprinted Polymers

Margaux Frigoli,* Joseph W. Lowdon, Nicolas Donetti, Robert D. Crapnell, Craig E. Banks, Thomas J. Cleij, Hanne Diliën, Kasper Eersels, and Bart van Grinsven

Cite This: *ACS Omega* 2024, 9, 36411−36420

Read Online

ACCESS | Metrics & More | Article Recommendations | Supporting Information

ABSTRACT: *Pseudomonas aeruginosa* is a multidrug-resistant Gram-negative bacterium that poses a significant threat to public health, necessitating rapid and on-site detection methods for rapid recognition. The goal of the project is therefore to indirectly detect the presence of *P. aeruginosa* in environmental water samples targeting one of its quorum-sensing molecules, namely, (*S*)-*N*-butyryl homoserine lactone (BHL). To this aim, molecularly imprinted polymers (MIPs) were synthesized via bulk free-radical polymerization using BHL as a template molecule. The obtained MIP particles were immobilized onto screen-printed electrodes (MIP-SPEs), and the BHL rebinding was analyzed via electrochemical impedance spectroscopy (EIS). To study the specificity of the synthesized MIPs, isotherm curves were built after on-point rebinding analysis performed via LC−MS measurements for both MIPs and NIPs (nonimprinted polymers, used as a negative control), obtaining an imprinting factor (IF) of 2.8 (at C_f = 0.4 mM). The MIP-SPEs were integrated into an electrochemical biosensor with a linear range of 1×10^1−1×10^3 nM and a limit of detection (LoD) of 31.78 ± 4.08 nM. Selectivity measurements were also performed after choosing specific interferent molecules, such as structural analogs and potential interferents, followed by on-point analysis performed in spiked tap water to prove the sensor's potential to detect the presence of the quorum-sensing molecule in environmentally related real-life samples.

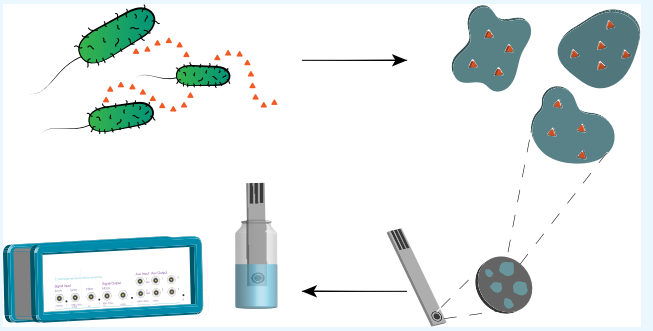

INTRODUCTION

Bacterial contamination poses a significant challenge in the healthcare industry, leading to numerous illnesses and fatalities.[1] The World Health Organization (WHO) recognized the severity of the issue and, in 2017, published a catalog identifying 12 families of bacteria considered to be the greatest threat to human health.[2] This catalog highlighted the danger posed by Gram-negative bacteria that developed antibiotic resistance, with multidrug-resistant *Pseudomonas aeruginosa* being one of the bacteria present within the list. *P. aeruginosa* is commonly found in soil, water, and vegetation and is particularly dangerous for hospitalized patients, causing urinary and respiratory tract infections.[3−5] Therefore, the urgency to address bacterial contamination, especially with antibiotic-resistant strains, has encouraged the exploration of novel detection methods.[6,7]

Different types of technologies have been developed for the detection of the pathogen, most of them being focused on the recognition of the whole microorganism.[8] The methods based on whole-cell detection started with culture-based analysis performed in qualified laboratories, a process that can take up to 7 days before the infection is detected or the pathogen is identified.[9] On the other hand, pathogenic cells were also successfully implemented into biosensors, namely, devices able to detect a specific target and generate a signal through the corresponding transducer coupled to the sensor itself.[10] In this category fall, for instance, the so-called surface-imprinted polymers (SIPs), which in the last years have gained increasing interest in the scientific world.[11] However, the main drawback associated with this approach lies in the need to handle dangerous pathogens during the sensing material preparation process.[12] This also leads to a lack of scalability and reproducibility; thus, effective procedures to produce them on a bigger scale still have to be found.[13] Alternatively, novel biosensors have emerged as a promising solution, detecting specific small molecules related to the bacteria metabolism instead of targeting the whole microorganism.[14]

Received: April 25, 2024
Revised: July 9, 2024
Accepted: July 29, 2024
Published: August 14, 2024

Among the novel technologies introduced in the field of biosensors, molecularly imprinted polymers (MIPs) represent a technology that has been demonstrated to be a solid alternative for the detection of a wide variety of contaminants thanks to their tunability, versatility, and ease of preparation.[15,16] MIPs are smart materials constituted by a polymer matrix, and one of the ways to synthesize them is via the free-radical polymerization of monomers and cross-linkers in a specific solvent mediated by a thermal/photo initiator.[17] There are multiple ways to prepare MIPs, including bulk, precipitation or emulsion polymerization, and solid-phase synthesis, and recent advances also introduced the possibility of synthesizing MIPs via direct electropolymerization on the surface of electrodes.[18−21] However, among all the available methods, in this work, the MIP particles were prepared via bulk polymerization, which is one of the cheapest and most straightforward approaches available.[22] In this scenario, an innovative approach for pathogenic bacteria detection involves targeting metabolites or toxins secreted by the bacteria themselves, enabling the indirect detection of the microorganism through its mainly used small molecules.[23−25] The quorum sensing system of the *P. aeruginosa* species, used for the cell-to-cell communication system, is highly suitable as a target for biosensing as it produces molecules that can be attributed to the presence of bacteria in a sample.[26−28] The molecule (*S*)-*N*-butyryl-L-homoserine lactone (BHL) is a key component of this system and was therefore identified as a suitable target for indirect detection of Gram-negative bacteria such as *P. aeruginosa*.[29,30] From a biological point of view, the detection of this compound is highly interesting as it has been demonstrated that the presence of quorum-sensing molecules in water lines contaminated with *P. aeruginosa* plays an essential role in the potential pathogenesis of these species.[31] To date, research efforts have been made mainly to use AHL-based quorum sensing molecules to inhibit the biofilm synthesis of certain bacteria strains, but there are still only a few examples of the use of BHL as a template for sensing purposes.[32−35]

The aim of this project was therefore to develop an MIP-based electrochemical sensor for the direct detection of BHL in drinking water samples. The MIPs were mixed with carbon ink for the construction of screen-printed electrodes (SPEs), which are low-cost and versatile materials that allow for impedimetric measurements with electrochemical impedance spectroscopy (EIS). This approach minimizes the need for handling live pathogens, enhances safety, and allows for a more efficient, reproducible, large-scale production of low-cost, fast sensors for bacterial identification.

MATERIALS AND METHODS

Materials. (*S*)-(−)-α-Amino-γ-butyro lactone hydrobromide (99%), ethylene glycol dimethacrylate (98%), 2,2′-azobis(2-methyl propionitrile) (98%), sodium carbonate (99.5%), sodium bicarbonate (99.5%), sodium hydroxide (99%), anhydrous dichloromethane (99.8%), dichloromethane (99.8%), triethylamine (99.5%), acrylamide (≥99%), methacrylic acid (99.5%), trimethylolpropanetrimethacrylate, acetic acid (99%), *m*-dihydroxybenzene (99%), 2-benzofuran-1,3-dione (99%), methanesulfonic acid (98%), hydrochloric acid (37%), and 2-methylprop-2-enoyl chloride (97%) were purchased from Sigma-Aldrich. Methanol (99%), butyryl chloride (99%), magnesium sulfate (99.5%), and dimethyl sulfoxide (99%) were purchased from Fisher Scientific. Additionally, hexane (>99%) and chloroform (>99%) were purchased from BioSolve. All of the solutions used for the MIP and NIP rebinding experiments were prepared using ultrapure water with a resistivity of 18.2 MΩ cm^{-1}.

General Equipment. LC−MS analysis was performed using an LCMS-2020 instrument from Shimadzu analyzing the single ion found at a m/z of 172.19 $[M + H]^+$. NMR analyses were performed using a 400 MHz Year Hold Superconducting Magnet (400JJYH) from Jeol Ltd. The impedance analyzer was purchased from Zurich Instruments (S/N: MF-DEV4891). The software used for the data analysis and picture production were Origin 2021b, ChemDraw 20.0, Zurich Instruments LabOne, MestRe Nova x64, and Adobe Illustrator 2023.

Synthesis of (*S*)-*N*-Butyryl Homoserine Lactone (BHL). (*S*)-*N*-butyryl homoserine lactone (BHL) was synthesized following a reported procedure.[36] In short, a mixture of (*S*)-(−)-α-amino-γ-butyro lactone hydrobromide (**1**) (1.3 equiv, 13.75 mmol, 2.5 g) and sodium carbonate (2.6 equiv, 27.5 mmol, 2.92 g) was prepared. Water (50 mL) and dichloromethane (50 mL) were added to the flask under vigorous stirring at room temperature. Butyryl chloride (**2**) (1 equiv, 10.58 mmol, 1.1 mL) was then added dropwise, and the reaction was stirred for 2 h at room temperature. The organic and aqueous phases were separated, and the latter was extracted with dichloromethane (2 × 100 mL). The combined organic phases were then washed with a saturated solution of sodium bicarbonate (2 × 100 mL) and dried with magnesium sulfate, and the solvent was removed under reduced pressure to obtain a white solid. The obtained powder was purified with Biotage coupled with an evaporative light scattering detector (ELSD). A gradient going from 1 to 9% methanol in DCM was used. LC−MS and NMR analyses were performed to assess the product's purity. The obtained spectra (Figures S1−S3) and chromatograms were consistent with earlier work and literature.[37] The final product (**3**) was obtained as a white powder and stored at 8 °C (635 mg, y = 41%) (Figure 1). The stereoselectivity was maintained as reported in previous studies.[36]

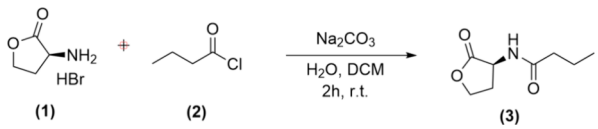

Figure 1. Schematic representation of the synthesis of BHL.

Synthesis of Molecularly Imprinted Polymers. Molecularly imprinted polymers (MIP) and nonimprinted polymers (NIP) were made using a free-radical polymerization process executed through a bulk polymerization technique (Figure S4). MIPs and NIPs were always synthesized in parallel using the same materials and quantities, with the only difference being the absence of the template molecule in the NIP sample. After dissolving the template molecule (BHL, 0.29 mmol, 50 mg, 1 equiv) in the chosen solvent (DMSO, 4 mL), the monomer (MAA, 1.17 mmol, 98.5 μL, 4 equiv) and cross-linker (EGDMA, 3.54 mmol, 660.1 μL, 12 equiv) were added to the glass vial, and the resulting solutions were sonicated for 2 min to allow the formation of the prepolymerization mixtures. Consequently, the radical initiator (AIBN, 0.292 mmol, 48 mg, 1 equiv) was added, and then the mixtures were degassed with nitrogen for 10 min to remove any oxygen present. The glass vials were then sealed, placed in an oil bath preheated at 65 °C,

https://doi.org/10.1021/acsomega.4c03970
ACS Omega 2024, 9, 36411−36420

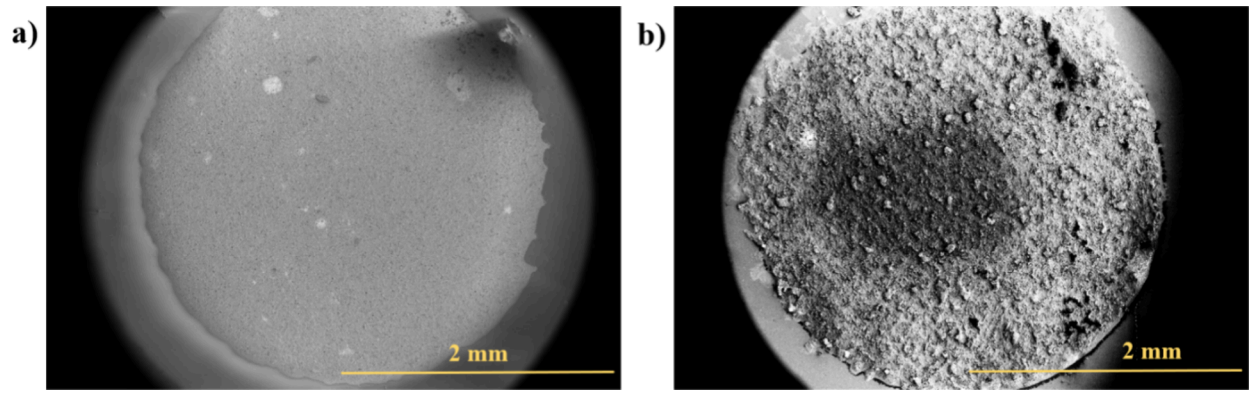

Figure 2. Scanning electron microscopy characterization of the screen-printed electrodes' surface of the (a) bare SPE and (b) MIP-functionalized SPE.

and left overnight. The resulting bulk polymers were crushed, washed with methanol (2 × 20 mL), and dried in the oven for 3 h at 70 °C. Subsequently, the dry MIP and NIP chunks were crushed using a mortar to obtain a fine powder, which was then extracted using two Soxhlet cycles overnight to remove any unreacted material and to create the free cavities by extracting the template still trapped in the MIP particles. The first cycle used a solvent mixture of AcOH/MeOH (1:9, 1 × 250 mL), whereas the second extraction was performed with methanol only (1 × 250 mL). After the extraction process, the powders were dried at 65 °C in an oven overnight and then precisely weighed to perform the rebinding analysis.

Rebinding Analysis via LC−MS. To analyze the recognition and rebinding capacity of the MIPs and NIPs, samples were prepared by weighing 10 mg of MIP and NIP powder in a glass vial for every concentration chosen, and an extra vial was prepared after every synthesis to check whether the material was leaching and ensure that the extraction was successful. Subsequently, 10 solutions at different concentrations (0.005−1 mM) were prepared using ultrapure water. The vials containing the powders and 2.5 mL of BHL solutions were allowed to rebind on a shaking plate set at 190 rpm for 90 min, then filtered and analyzed with LC−MS. To analyze the rebinding properties of the template, a calibration curve was created before every rebinding experiment using the same solutions and analyzing the instrument response at 172.19 m/z $[M + H]^+$.

Screen-Printed Electrode Fabrication. Stencil designs using a microDEK 1760RS screen-printing apparatus (DEK, Weymouth, UK) were employed in the fabrication of the screen-printed electrodes (SPEs). Initially, a carbon-graphite ink formulation was applied to a polyester flexible film (Autostat, 250 μm thickness) through the screen-printing process. Subsequently, the deposited layer underwent curing at 60 °C for 30 min in a ventilated oven. Following this, a silver/silver chloride (60:40) reference electrode was screen-printed using Ag/AgCl paste (Product Code: C2040308P3; Gwent Electronic Materials Ltd., UK) onto the plastic substrate and similarly cured at 60 °C for 30 min. Lastly, an insulating dielectric paste ink (Product Code: D2070423D5; Gwent Electronic Materials Ltd., UK) was applied to shield the connections and delineate the 3.1 mm diameter graphite working electrode. Once again, this layer underwent curing under the same conditions as those for the preceding layers. Upon completion of these procedures, the SPEs were prepared for use, with their characteristics extensively documented in prior research.[38−40]

Rebinding Analysis via Electrochemical Impedance Spectroscopy (EIS). The rebinding analysis to assess the fabricated MIP-SPEs and NIP-SPEs performance was performed using an impedance analyzer purchased from Zurich Instruments with an adaptor for screen-printed electrodes. The solutions at increasing concentrations (1×10^1 to 1×10^3 nM) were prepared in ultrapure water using the previously synthesized BHL molecule. Consequently, 5 mL of each solution was placed in glass vials so that the electrodes could easily be dipped in the solutions. After stabilization of 10 min in phosphate-buffered saline (PBS) to record a baseline, the electrode was dipped in solutions at increasing BHL concentrations for 10 min each, and the impedance was recorded. The analysis was performed in a broad frequency range (10−100 000 Hz), and the data were analyzed at a unique frequency corresponding to a phase angle of 45°.

RESULTS AND DISCUSSION

Characterization with Scanning Electron Microscope (SEM). To understand the characteristics and properties of the polymer particles and of the screen-printed electrodes used throughout this study, specific analyses were performed using scanning electron microscopy (SEM) coupled with an energy-dispersive X-ray detector (EDX or EDS). This characterization process clarified the dimensions and chemical properties of the particles obtained after the free-radical polymerization process performed by applying the bulk polymerization method, thus resulting in heterogeneously dispersed particles that tend to form agglomerates (Figure S5). The polymer particles obtained were measured and ranged in size from 0.2 to 5 μm for both MIPs and NIPs. Furthermore, the EDS confirmed the elemental composition of the MIPs and NIPs, with the higher peak of carbon also attributed to the conductive tape used to immobilize the particles onto the sample holder (Figure S5). The apparent excitation band relating to gold is obtained from the preparation of the SEM sample by sputtering.

Furthermore, the screen-printed electrodes were also characterized to study the difference between the non-functionalized SPE and the MIP-SPE. As it is possible to see in Figure 2a, the bare electrode surface is covered with carbon-graphitic ink that does not contain MIP and NIP particles, resulting in a more homogeneous layer. On the other hand, the

https://doi.org/10.1021/acsomega.4c03970
ACS Omega 2024, 9, 36411−36420

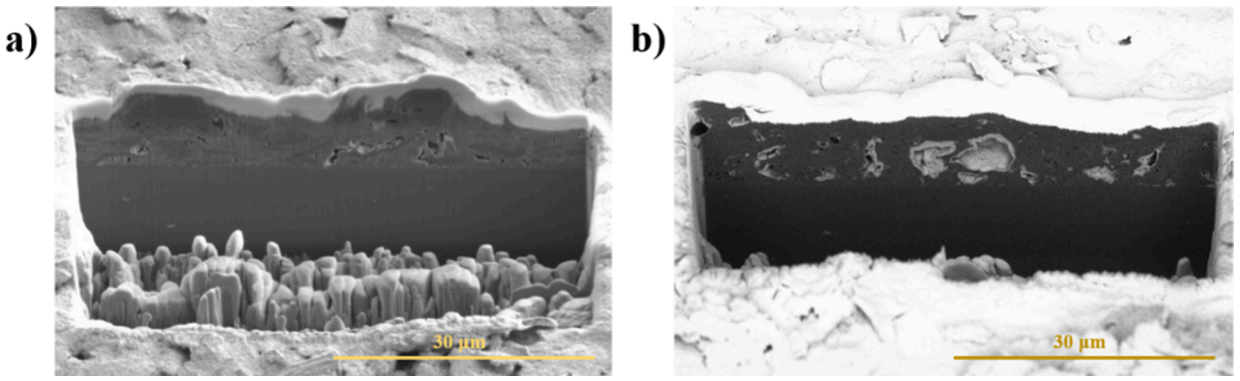

Figure 3. Scanning electron microscopy characterization of the electrode layers of the (a) bare SPE and (b) functionalized SPE.

MIP-SPE picture clearly shows the presence of particles that protrude from the surface (Figure 2b).

The screen-printed electrodes were further characterized using an ion beam scanning electron microscope (FIB-SEM).[41] This technology made it possible to cut the SPEs to image the surface at a very fine scale, allowing for precise cross-sectioning and measurement of the thickness of the upper layer of the electrodes (Figure 3). After coating the samples with platinum to enhance the conductivity and to avoid sample spoilage during the process, the samples were cut with an angle of 90° to ensure deep penetration within the layers. The result shows that the bare SPE does not contain polymer particles, whereas the MIP-SPE clearly shows the presence of particles also within the ink layer. Moreover, the calculation of the thickness of the layers of bare and functionalized SPEs was performed, which was found to be 7.03 ± 1.54 μm. Emphasizing that the overall thickness of the two samples is similar is crucial given that the primary distinction lies in the presence (functionalized) or absence (bare) of MIP and NIP particles within the carbon-graphitic ink and not in the manufacturing process. Further characterization with X-ray diffraction (XRD) was also performed. Nonetheless, because of the high amount of graphitic ink compared to the MIP powder, this technique did not offer valuable insights in terms of surface characterization, showing mainly that the presence of graphite diffraction tends to cover the signals coming from the MIP polymeric matrix (Figure S9).

Rebinding Analysis via LC−MS. In this study, 26 different MIP and NIP compositions were synthesized and tested by using different types and combinations of monomer, cross-linker, and solvent. The materials used were methacrylic acid (MAA), ethylene glycol dimethacrylate (EGDMA), and dimethyl sulfoxide (DMSO), and a few syntheses were also made with chemicals such as trimethylolpropane trimethacrylate (TRIM), acrylamide (AM), and chloroform (Table S1). This empirical study was done to understand how different functional groups and interactions influence the polymer−template affinity; for instance, what is the effect of changing the cross-linker from a structure containing two double bonds (EGDMA) to one containing three (TRIM), or for instance, what is the rebinding affinity of the template when the polymer is synthesized with an acidic monomer (MAA) or a nonacidic one (AM). However, the materials that gave the best results were methacrylic acid (MAA) and ethylene glycol dimethacrylate (EGDMA), and the best ratio was found to be 1:4:12 (BHL/MAA/EGDMA). EGDMA is highly compatible with MAA because they both have methacrylate groups to polymerize, and if on one side MAA can generate strong hydrogen bonding with the template, EGDMA is responsible for maintaining the structural rigidity of the polymeric matrix. The use of EGDMA in combination with MAA for creating MIPs has been widely reported in the literature, highlighting its effectiveness in forming robust, high-affinity polymers for various target molecules.[42,43] To study the potential of the synthesized MIP particles to rebind to (*S*)-*N*-butyryl homoserine lactone (BHL), specific analyses were performed using the liquid chromatography−mass spectrometry (LC−MS) technique, as reported in the Materials and Methods section. Two parameters were analyzed to assess the rebinding properties of the MIPs, namely, the imprinting factor (IF) and the binding capacity (Sb). The IF is a parameter used to measure the binding affinity of the template to the MIP cavities by comparing the amount of template bound after rebinding to the MIP with the corresponding NIP (eq 1).

$$\text{Imprinting factor (IF)} = \frac{\text{binding capacity (MIP) at } X \text{ mM}}{\text{binding capacity (NIP) at } X \text{ mM}} \quad (1)$$

The imprinting factor gives information on the specificity of the MIP by applying a direct comparison with the negative control, the NIP. If the resulting value is significantly higher than 1, this means that the MIP presents specific binding sites able to selectively detect the target molecule, whereas a value lower than 1 corresponds to a prevalence of nonspecific interactions of the template with the functional groups of the polymer. On the other hand, the binding capacity (Sb) is a parameter that shows the amount of target molecules that can bind to the MIP/NIP, and it is often influenced by the accessibility of the template to the binding sites and by the concentrations used (eq 2).

$$\text{Binding capacity (Sb)} = \frac{((C_i - C_f) * Q_s)}{Q_m} \quad (2)$$

In this equation, the final concentration (C_f) is calculated by starting from the initial concentration (C_i) using the calibration curve. The result is multiplied by the quantity of BHL added (Q_s) and divided by the amount of MIP-NIP used for the rebinding experiments (Q_m). The obtained data were plotted and fitted asymptotically to understand the dynamics of the system, thus obtaining the corresponding binding isotherms (Figure 4).

Table S1 shows all the data gathered from the rebinding measurements performed on the synthesized MIPs, showing that some combinations of monomers and cross-linkers gave

https://doi.org/10.1021/acsomega.4c03970
ACS Omega 2024, 9, 36411−36420

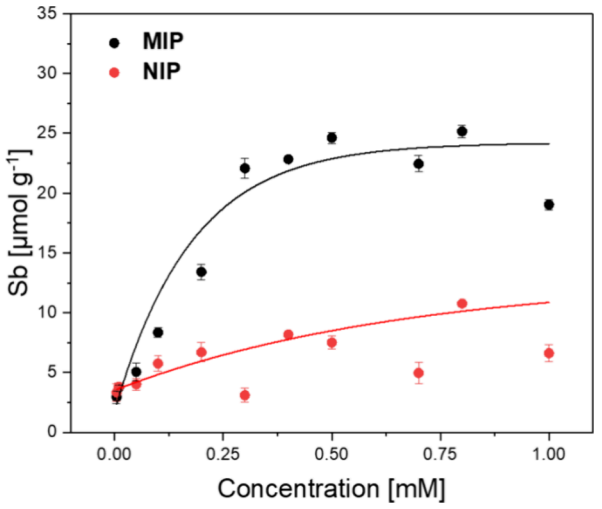

Figure 4. Rebinding isotherms of MIP (black line, R^2 = 0.935) and NIP (red line, R^2 = 0.737) at increasing concentrations.

inconsistent results or did not polymerize (i.e., MIP10, MIP11), or the imprinting factor was not high enough to be considered specific (i.e., MIP05, MIP14), or again the Sb was insufficiently intense (i.e., MIP15). Therefore, MIP17 was selected as the best material thanks to its IF and Sb, and it was synthesized and tested again using 10 concentrations instead of 6 to ensure the quality of the results. As a result, MIP17 showed high specificity, presenting an average imprinting factor equal to 2.80 (at 0.4 mM) and an Sb equal to 25.1 μmol g^{-1} (Figure 4). Furthermore, the results show that the nonimprinted polymer presents highly diverse responses to the different concentrations used, mainly due to the fact that the template can only form nonspecific interactions with the functional groups on the polymer surface instead of exploiting the lock-and-key mechanism present in the molecularly imprinted polymer cavities. This can be explained by the fact that the formation of oriented cavities that mimic the shape and interactions of the template can enhance the binding capacities of the target molecule itself during the rebinding with the MIP (Figure S6).[44−46]

Screen-Printed Electrodes Functionalized with MIPs. The MIP and NIP screen-printed electrodes (MIP-SPEs and NIP-SPEs) were obtained by modifying the carbon-graphitic ink by mixing the polymer particles previously synthesized with the ink itself. This was carried out using 5% (wt) of MIP or NIP particles in the ink, where the percentage was selected thanks to previous studies that demonstrated the consistency of the procedure.[47,48] The resulting mixture was screen-printed on top of the carbon-graphite working electrode to create the final SPEs with a connection length of 32 mm and an average resistance of 2.16 ± 0.06 Ω.[49] The obtained SPEs were used to perform impedimetric measurements via electrochemical impedance spectroscopy (EIS) by dipping the fabricated sensor in phosphate-buffered saline (PBS) solutions with increasing concentrations of the template molecule in the range from 1×10^1 to 1×10^3 nM and analyzing the impedimetric response during a 10 min time interval.[50,51] As a result, an impedimetric profile was obtained (Figure 5a). Consequently, a dose−response curve was generated using data obtained from triplicate analyses. The mean impedance values associated with various BHL concentrations were normalized for different time periods. These absolute values were then plotted against the BHL concentrations using Origin, resulting in a graph that shows the change in absolute impedance (y axis) in response to different BHL concentrations (x axis) (Figure 5b).

The data were fitted allometrically ($y = ax^b$) because this function is one of the most widely used when impedimetric data after rebinding experiments are plotted.[52,53] The corresponding Bode and Nyquist plots for the rebinding analysis of the target molecule to the MIP-SPE are also reported (Figure S8). As a result, it is possible to see that the MIP-SPE sensor has a good specificity compared to the negative control (NIP-SPE), with the limit of detection (LoD) calculated with the 3σ method being equal to 31.78 ± 4.08 nM, thus proving the potential of the sensor to detect the quorum sensing molecules also in very diluted samples such as tap water, drinking water, wastes, or irrigation water.[54] The result is particularly promising especially if compared to other similar research where higher LoDs were obtained.[55−57] Moreover, the low standard deviation obtained within the

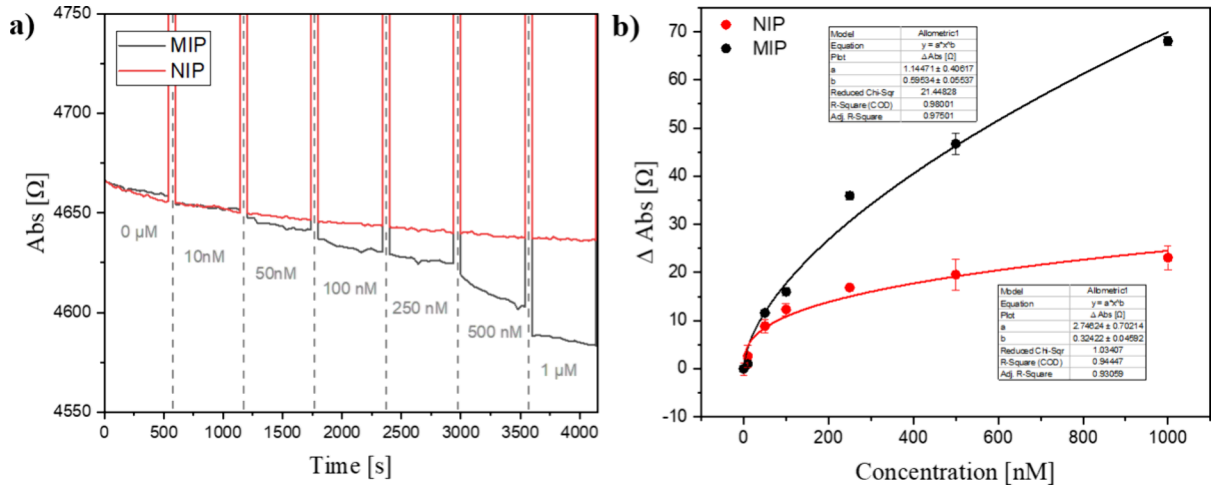

Figure 5. Impedimetric measurements performed to assess the MIP-SPE and NIP-SPE response to increasing concentrations of BHL (1 nM−1 μM). (a) Absolute impedance profiles for MIP (black line) and NIP (red line). (b) Dose−response curves obtained from the delta of the absolute impedance for MIP-SPE (black line) and NIP-SPE (red line).

https://doi.org/10.1021/acsomega.4c03970
ACS Omega 2024, 9, 36411−36420

data and the stability of the EIS signal further prove the feasibility of these measurements in water-based samples. Studies on the isolated MIP and MIP-SPE indicate that the presence of graphite ink does not significantly obstruct the complementary binding pocket of the MIP. This suggests that the suggested bonding interactions within the receptor remain robust enough to effectively bind and detect BHL.[58] Moreover, the distinct performance difference between MIP and NIP implies that the graphite ink used as a binder for the SPE is sufficiently porous, allowing for the diffusion of BHL molecules into the material without hindering the binding process. Previous studies utilizing this approach have demonstrated that polymeric receptors can work synergistically with the screen-printing methodology, resulting in highly versatile and sensitive biosensors.[59,60]

The electrochemical surface area of both the functionalized (ECSA_F) and nonfunctionalized screen-printed electrodes (ECSA_NF) was also calculated using the $[Fe(CN)_6]^{3-/4-}$ redox probe. Such a calculation was done using the Randles–Ševćik equation (eq 3), where i_p is the maximum value of the current (A), n is the number of electrons transferred in the reaction, D is the diffusion coefficient ($cm^2\ s^{-1}$), C is the concentration (mol/cm^3), and v is the scan rate ($V\ s^{-1}$), and a constant with a value of 2.69×10^5 is also included because the solution is at a temperature equal to 25 °C.

$$\mathrm{ECSA} = \frac{i_p}{2.69 \times 10^5 n_2^3 C \sqrt{Dv}} \quad (3)$$

The results obtained from the equation are summarized in Table 1, whereas all of the calculations and plots obtained are shown in the Supporting Information (Figure S7).

Table 1. Calculated Electrode Areas (ECSAs) for the Bare and Functionalized Screen-Printed Electrodes via the Randles–Ševćik Equation

	i_p(A)	ECSA (cm^2)
nonfunctionalized SPE	1.54×10^{-4}	1.93E-02
functionalized SPE	2.36×10^{-4}	2.36E-02

As expected, the calculations reveal that the electrochemically active surface area of the electrodes is higher for the functionalized electrode in comparison to that of the nonfunctionalized bare electrode. This can be explained by the fact that the MIP-SPEs, after the implementation of the MIP particles mixed with the ink, carry binding sites that increase the roughness of the material. This, in turn, leads to an increase in the total calculated active area, resulting in data that are consistent with previously reported literature.[61,62]

Selectivity Measurements. Once the sensitivity and specificity of the sensor are determined, the selectivity also has to be studied to properly understand the sensor's behavior. To prove the sensor's selectivity, specific molecules were chosen to perform impedimetric measurements at the interface using the same concentration range and the same methodology used for the dose–response curve analysis to be able to precisely compare the obtained results. In particular, the first molecule chosen was a structural analogue of BHL, namely, (*S*)-(−)-α-amino-γ-butyro lactone hydrobromide (ABL), to check the sensor's response to molecules bearing almost the same structure. Moreover, ascorbic acid was chosen because its form also presents similarities with the template thanks to its five-membered ring structure and it is a possible contaminant that can be present in water. For the same reason, glucose was selected as the last molecule for this selectivity study because it is a very widespread contaminant that can be present in a variety of samples, ranging from tap and river water to food and biological samples. The results show that the sensor presents good selectivity toward the target molecule (BHL), represented with a black line, compared to the chosen interferent molecules (Figure 6). In particular, the sensor shows a very low response to ascorbic acid and glucose, namely, molecules that are likely to be present as interferents. On the other hand, the sensor shows a higher response to ABL; besides, the response is still lower compared to the one of the actual targets, showing that the extra carbonyl group added to the molecule after the synthesis plays a key role in the rebinding of the BHL molecule. Furthermore, ABL is an interferent molecule that cannot be present in any sample; thus, it does not represent any risk of cross-contamination.

Real-Life Sample Analysis. The last step of this research was aimed at proving the working principle of the prepared

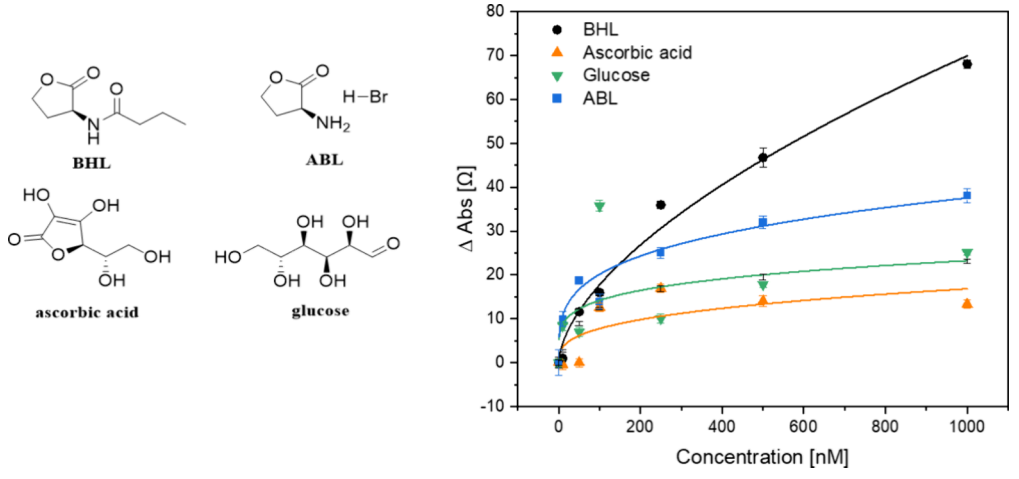

Figure 6. Dose–response curves extrapolated from EIS measurements after exposure to the MIP-SPEs to increasing concentrations of interferent molecules (1 nM–1 μM), namely, ascorbic acid (orange line), glucose (green line), (*S*)-(−)-α-amino-γ-butyro lactone hydrobromide (blue line), and BHL (black line).

https://doi.org/10.1021/acsomega.4c03970
ACS Omega 2024, 9, 36411–36420

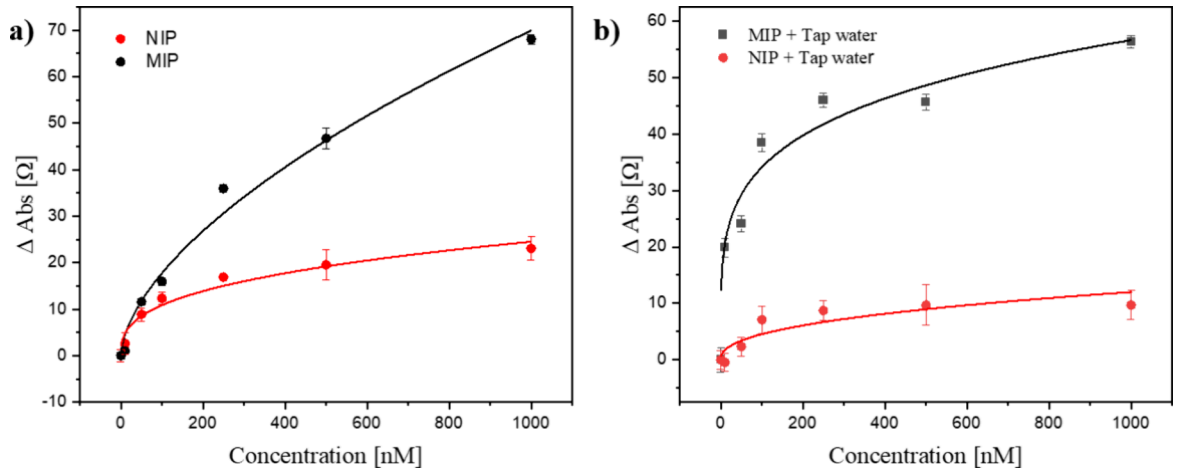

Figure 7. Impedimetric real-life sample analysis in (a) PBS and (b) tap water at increasing concentrations of BHL (1 nM−1 μM).

MIP-SPE sensor in a real-life sample. In the last years, one of the main bacterial contamination problems was related to the infections spread through tap water involved in the food industry for beverage preparation or also to irrigation water, therefore, the chosen real-life sample was unfiltered tap water.[1,63,64] In particular, impedimetric measurements were performed by spiking the unfiltered tap water samples with the template, namely, the *N*-butyryl homoserine lactone quorum sensing molecule (BHL), and the resulting solution was then converted into a PBS solution by dissolving PBS tablets in it. This step is fundamental to ensure compatibility with the previous results and because impedimetric measurements cannot be performed in solutions that do not contain electrolytes. To properly compare the results, the analysis of the real-life samples was performed also with the negative control material, namely, the NIP-SPE. The analysis was performed in the same concentration range used to study the sensor's specificity (1×10^1−1×10^3 nM), and the resulting difference in absolute impedance for MIP-SPE and NIP-SPE is illustrated for the measurements performed in both ultrapure buffer solution (Figure 7a) and spiked tap water (Figure 7b).

The results show interesting aspects of the sensor's performance, and they prove that the sensor can detect the presence of quorum-sensing molecules in tap water with a limit of detection (LoD) of 7.99 ± 1.17 nM. Remarkably, the sensor demonstrated to be able to present a higher imprinting factor in tap water (4.71) than in ultrapure water (2.37), and a possible explanation of this could be due to the presence of ions (i.e., Ca^{2+} or Mg^{2+}) that could potentially chelate to the MIP-SPE and NIP-SPE functional groups reducing nonspecific target binding.[65] This observation can be supported by the overall difference of maximum impedance for the MIP-SPEs in tap water and pure buffer solution (56.29 and 68.04 Ω, respectively) and for the NIP-SPEs (9.69 and 23.08 Ω, respectively). Additionally, the fact that the measurement tends to level off at a concentration of 1 μM further highlights that the ions present in the sample could interfere with the binding process; nonetheless, the calculated LoD was found to be in the same magnitude range. Overall, the analyses performed show that the sensor can detect the presence of small quantities of quorum-sensing molecules in unfiltered tap water, opening the way for the possibility of finding bacterial contamination earlier in different kinds of water-based samples, including irrigation water or tap water used inside hospitals.

CONCLUSIONS

This manuscript presents the development of screen-printed electrodes functionalized with molecularly imprinted polymers (MIPs) for the precise detection of the (*S*)-*N*-butyryl homoserine lactone (BHL) quorum sensing molecule, which is crucial in *Pseudomonas aeruginosa* communication. Through refining MIP composition, the sensor exhibits high specificity and good selectivity for BHL detection, showcasing the potential for real-world applications in water quality monitoring. Future research should focus on enhancing the sensor's design for wider application in portable devices, advancing point-of-care detection systems for diverse environmental contexts, and improving accessibility in resource-constrained settings.

ASSOCIATED CONTENT

Supporting Information

The Supporting Information is available free of charge at https://pubs.acs.org/doi/10.1021/acsomega.4c03970.

LC−MS analysis; ^{1}H NMR and ^{13}C NMR spectra; schematic representation of the synthesis and rebinding of MIPs; SEM characterization; materials tested for MIPs; template−polymer interaction scheme; and ECSA, Bode and Nyquist, and XRD data (PDF)

AUTHOR INFORMATION

Corresponding Author

Margaux Frigoli − *Sensor Engineering Department, Faculty of Science and Engineering, Maastricht University, Maastricht 6200 MD, The Netherlands;* orcid.org/0000-0001-8543-741X; Email: m.frigoli@maastrichtuniversity.nl

Authors

Joseph W. Lowdon − *Sensor Engineering Department, Faculty of Science and Engineering, Maastricht University, Maastricht 6200 MD, The Netherlands*

Nicolas Donetti − *Sensor Engineering Department, Faculty of Science and Engineering, Maastricht University, Maastricht 6200 MD, The Netherlands*

Robert D. Crapnell − *John Dalton Building, Faculty of Science and Engineering, Manchester Metropolitan University, Manchester M1 5GD, U.K.*

https://doi.org/10.1021/acsomega.4c03970
ACS Omega 2024, 9, 36411−36420

Craig E. Banks − *John Dalton Building, Faculty of Science and Engineering, Manchester Metropolitan University, Manchester M1 5GD, U.K.;* orcid.org/0000-0002-0756-9764
Thomas J. Cleij − *Sensor Engineering Department, Faculty of Science and Engineering, Maastricht University, Maastricht 6200 MD, The Netherlands;* orcid.org/0000-0003-0172-9330
Hanne Diliën − *Sensor Engineering Department, Faculty of Science and Engineering, Maastricht University, Maastricht 6200 MD, The Netherlands*
Kasper Eersels − *Sensor Engineering Department, Faculty of Science and Engineering, Maastricht University, Maastricht 6200 MD, The Netherlands;* orcid.org/0000-0002-0214-1320
Bart van Grinsven − *Sensor Engineering Department, Faculty of Science and Engineering, Maastricht University, Maastricht 6200 MD, The Netherlands;* orcid.org/0000-0002-6939-0866

Complete contact information is available at: https://pubs.acs.org/10.1021/acsomega.4c03970

Notes

The authors declare no competing financial interest.

■ ACKNOWLEDGMENTS

This work was supported by the European Regional Development Fund through the AgrEU food project funded by the Interreg VA Flanders-The Netherlands program, CCI grant 2014TC16RFCB046.

■ REFERENCES

(1) Crone, S.; Vives-Flórez, M.; Kvich, L.; Saunders, A. M.; Malone, M.; Nicolaisen, M. H.; Martínez-García, E.; Rojas-Acosta, C.; Catalina Gomez-Puerto, M.; Calum, H.; Whiteley, M.; Kolter, R.; Bjarnsholt, T. The environmental occurrence of Pseudomonas aeruginosa. *Apmis* **2020**, *128*, 220−231.
(2) *WHO publishes list of bacteria for which new antibiotics are urgently needed*, (n.d.). https://www.who.int/news/item/27-02-2017-who-publishes-list-of-bacteria-for-which-new-antibiotics-are-urgently-needed 2017.
(3) Rossi, E.; La Rosa, R.; Bartell, J. A.; Marvig, R. L.; Haagensen, J. A. J.; Sommer, L. M.; Molin, S.; Johansen, H. K. Pseudomonas aeruginosa adaptation and evolution in patients with cystic fibrosis. *Nat. Rev. Microbiol.* **2021**, *19*, 331−342.
(4) Garcia-Clemente, M.; de la Rosa, D.; Máiz, L.; Girón, R.; Blanco, M.; Olveira, C.; Canton, R.; Martinez-García, M. A. Impact of pseudomonas aeruginosa infection on patients with chronic inflammatory airway diseases. *J. Clin. Med.* **2020**, *9*, 3800.
(5) Reynolds, D.; Kollef, M. The Epidemiology and Pathogenesis and Treatment of Pseudomonas aeruginosa Infections: An Update. *Drugs* **2021**, *81*, 2117−2131.
(6) Davies, J. C. Pseudomonas aeruginosa in cystic fibrosis: pathogenesis and persistence. *Paediatr. Respir. Rev.* **2002**, *3*, 128−134.
(7) Driscoll, J. A.; Brody, S. L.; Kollef, M. H. The epidemiology, pathogenesis and treatment of Pseudomonas aeruginosa infections. *Drugs* **2007**, *67*, 351−368.
(8) Hu, J.; Fu, K.; Bohn, P. W. Whole-Cell Pseudomonas aeruginosa Localized Surface Plasmon Resonance Aptasensor. *Anal. Chem.* **2018**, *90*, 2326−2332.
(9) e Silva, R. F.; Paixão, T. R. L. C.; Der Torossian Torres, M.; de Araujo, W. R. Simple and inexpensive electrochemical paper-based analytical device for sensitive detection of Pseudomonas aeruginosa. *Sens. Actuators B* **2020**, *308*, No. 127669.
(10) Tang, Y.; Ali, Z.; Zou, J.; Jin, G.; Zhu, J.; Yang, J.; Dai, J. Detection methods for Pseudomonas aeruginosa: history and future perspective. *RSC Adv.* **2017**, *7*, 51789−51800.
(11) Dar, K. K.; Shao, S.; Tan, T.; Lv, Y. Molecularly imprinted polymers for the selective recognition of microorganisms. *Biotechnol. Adv.* **2020**, *45*, No. 107640.
(12) Arreguin-Campos, R.; Jiménez-Monroy, K. L.; Diliën, H.; Cleij, T. J.; van Grinsven, B.; Eersels, K. Imprinted Polymers as Synthetic Receptors in Sensors for Food Safety. *Biosensors* **2021**, *11*, 46.
(13) Frigoli, M.; Lowdon, J. W.; Caldara, M.; Arreguin-Campos, R.; Sewall, J.; Cleij, T. J.; Diliën, H.; Eersels, K.; van Grinsven, B. Thermal Pyocyanin Sensor Based on Molecularly Imprinted Polymers for the Indirect Detection of *Pseudomonas aeruginosa*. *ACS Sens.* **2023**, *8*, 353.
(14) Chaplin, M. F. Biosensors. *Mol. Biol. Biotechnol.* **2021**, 357−393.
(15) Leibl, N.; Haupt, K.; Gonzato, C.; Duma, L. Molecularly Imprinted Polymers for Chemical Sensing: A Tutorial Review. *Chemosens.* **2021**, *9*, 123.
(16) Murugan, K.; Natarajan, A.; Rajaram, A. C. Halicacabum derived "turn-on-off" non-invasive molecularly imprinted polymer for selective profiling of 2-(3,4-dihydroxy phenyl) ethylamine in human fluid samples. *Microchem. J.* **2024**, *203*, No. 110862.
(17) Kaya, S. I.; Cetinkaya, A.; Ozkan, S. A. Molecularly imprinted polymers as highly selective sorbents in sample preparation techniques and their applications in environmental water analysis. *Trends Environ. Anal. Chem.* **2023**, *37*, No. e00193.
(18) Yang, H.; Liu, H. B.; Tang, Z. S.; Qiu, Z. D.; Zhu, H. X.; Song, Z. X.; Jia, A. L. Synthesis, performance, and application of molecularly imprinted membranes: A review. *J. Environ. Chem. Eng.* **2021**, *9*, No. 106352.
(19) Murugan, K.; Jothi, V. K.; Rajaram, A.; Natarajan, A. Novel Metal-Free Fluorescent Sensor Based on Molecularly Imprinted Polymer N-CDs@MIP for Highly Selective Detection of TNP. *ACS Omega* **2022**, *7*, 1368−1379.
(20) Murugan, K.; Natarajan, A. A novel N-CNDs/PAni modified molecular imprinted polymer for ultraselective and sensitive detection of ciprofloxacin in lentic ecosystems: a dual responsive optical sensor. *Anal. Methods* **2024**, *16*, 3413−3429.
(21) Frigoli, M.; Caldara, M.; Royakkers, J.; Lowdon, J. W.; Cleij, T. J.; Diliën, H.; Eersels, K.; van Grinsven, B. Gold screen-printed electrodes coupled with molecularly imprinted conjugated polymers for ultrasensitive detection of streptomycin in milk. *Microchem. J.* **2024**, *200*, No. 110433.
(22) Tabar, F. A.; Lowdon, J. W.; Caldara, M.; Cleij, T. J.; Wagner, P.; Diliën, H.; Eersels, K.; van Grinsven, B. Thermal determination of perfluoroalkyl substances in environmental samples employing a molecularly imprinted polyacrylamide as a receptor layer. *Environ. Technol. Innov.* **2023**, *29*, No. 103021.
(23) Rajkovic, A.; Jovanovic, J.; Monteiro, S.; Decleer, M.; Andjelkovic, M.; Foubert, A.; Beloglazova, N.; Tsilla, V.; Sas, B.; Madder, A.; De Saeger, S.; Uyttendaele, M. Detection of toxins involved in foodborne diseases caused by Gram-positive bacteria. *Compr. Rev. Food Sci. Food Saf.* **2020**, *19*, 1605−1657.
(24) Frigoli, M.; Lowdon, J. W.; Caldara, M.; Arreguin-Campos, R.; Sewall, J.; Cleij, T. J.; Diliën, H.; Eersels, K.; Van Grinsven, B. Thermal Pyocyanin Sensor Based on Molecularly Imprinted Polymers for the Indirect Detection of Pseudomonas aeruginosa. *ACS Sensors* **2023**, *8*, 353−362.
(25) Li, Y.; Zhu, J.; Zhang, H.; Liu, W.; Ge, J.; Wu, J.; Wang, P. High sensitivity gram-negative bacteria biosensor based on a small-molecule modified surface plasmon resonance chip studied using a laser scanning confocal imaging-surface plasmon resonance system. *Sensors Actuators B Chem.* **2018**, *259*, 492−497.
(26) Zhao, X.; Yu, Z.; Ding, T. Quorum-sensing regulation of antimicrobial resistance in bacteria. *Microorganisms* **2020**, *8*, 425.
(27) Capatina, D.; Feier, B.; Hosu, O.; Tertis, M.; Cristea, C. Analytical methods for the characterization and diagnosis of infection with Pseudomonas aeruginosa: A critical review. *Anal. Chim. Acta* **2022**, *1204*, No. 339696.

(28) Jiang, H.; Jiang, D.; Shao, J.; Sun, X. Magnetic molecularly imprinted polymer nanoparticles based electrochemical sensor for the measurement of Gram-negative bacterial quorum signaling molecules (N-acyl-homoserine-lactones). *Biosens. Bioelectron.* **2016**, *75*, 411−419.
(29) Rémy, B.; Plener, L.; Decloquement, P.; Armstrong, N.; Elias, M.; Daudé, D.; Chabrière, É. Lactonase Specificity Is Key to Quorum Quenching in Pseudomonas aeruginosa. *Front. Microbiol.* **2020**, *11*, 1−17.
(30) Kumar, L.; Patel, S. K. S.; Kharga, K.; Kumar, R.; Kumar, P.; Pandohee, J.; Kulshresha, S.; Harjai, K.; Chhibber, S. Molecular Mechanisms and Applications of N-Acyl Homoserine Lactone-Mediated Quorum Sensing in Bacteria. *Molecules* **2022**, *27*, 7584.
(31) Liu, J.; Sun, X.; Ma, Y.; Zhang, J.; Xu, C.; Zhou, S. Quorum Quenching Mediated Bacteria Interruption as a Probable Strategy for Drinking Water Treatment against Bacterial Pollution. *Int. J. Environ. Res. Public Health* **2020**, *17*, 9539.
(32) Bakaraki, N.; Chormey, D. S.; Bakirdere, S.; Engin, G. O. Development of a sensitive liquid−liquid extraction method for the determination of N-butyryl-L-homoserine lactone produced in a submerged membrane bioreactor by gas chromatography mass spectrometry and deuterated anthracene as the internal standard. *Anal. Methods* **2016**, *8*, 2660−2665.
(33) Acet, Ö.; Odabaşı, M. Detection of N-hexanoyl-L-homoserine lactone via MIP-based QCM sensor: preparation and characterization. *Polym. Bull.* **2023**, *80*, 6657−6674.
(34) Piletska, E. V.; Stavroulakis, G.; Larcombe, L. D.; Whitcombe, M. J.; Sharma, A.; Primrose, S.; Robinson, G. K.; Piletsky, S. A. Passive control of quorum sensing: Prevention of pseudomonas aeruginosa biofilm formation by imprinted polymers. *Biomacromolecules* **2011**, *12*, 1067−1071.
(35) Bakhti, S.; Saghabashi, A.; Sharafshadehi, S. A.; Rastmanesh, S.; Bostanghadiri, N.; Jalilpiran, A.; Fathi, J.; Shahraki, A. G.; Sameni, F. Biofilm Formation by Quorum Sensing and Manners to Deal It. *J. Med. Bacteriol.* **2024**, *12*, 54−67.
(36) Hodgkinson, J. T.; Galloway, W. R. J. D.; Casoli, M.; Keane, H.; Su, X.; Salmond, G. P. C.; Welch, M.; Spring, D. R. Robust routes for the synthesis of N-acylated-l-homoserine lactone (AHL) quorum sensing molecules with high levels of enantiomeric purity. *Tetrahedron Lett.* **2011**, *52*, 3291−3294.
(37) Flynn, P. B.; Busetti, A.; Wielogorska, E.; Chevallier, O. P.; Elliott, C. T.; Laverty, G.; Gorman, S. P.; Graham, W. G.; Gilmore, B. F. Non-thermal Plasma Exposure Rapidly Attenuates Bacterial AHL-Dependent Quorum Sensing and Virulence. *Sci. Reports* **2016**, *6*, 1−13.
(38) Galdino, F. E.; Foster, C. W.; Bonacin, J. A.; Banks, C. E. Exploring the electrical wiring of screen-printed configurations utilised in electroanalysis. *Anal. Methods* **2015**, *7*, 1208−1214.
(39) Khorshed, A. A.; Khairy, M.; Banks, C. E. Electrochemical determination of antihypertensive drugs by employing costless and portable unmodified screen-printed electrodes. *Talanta* **2019**, *198*, 447−456.
(40) Caldara, M.; Lowdon, J. W.; van Wissen, G.; Ferrari, A. G.; Crapnell, R. D.; Cleij, T. J.; Diliën, H.; Banks, C. E.; Eersels, K.; van Grinsven, B. Dipstick Sensor Based on Molecularly Imprinted Polymer-Coated Screen-Printed Electrodes for the Single-Shot Detection of Glucose in Urine Samples—From Fundamental Study toward Point-of-Care Application. *Adv. Mater. Interfaces* **2023**, *10*, 2300182.
(41) Nan, N.; Wang, J. FIB-SEM Three-Dimensional Tomography for Characterization of Carbon-Based Materials. *Adv. Mater. Sci. Eng.* **2019**, *2019*, 8680715.
(42) Yoshimi, Y.; Ohdaira, R.; Iiyama, C.; Sakai, K. Gate effect" of thin layer of molecularly-imprinted poly(methacrylic acid-co-ethyl-eneglycol dimethacrylate). *Sensors Actuators B Chem.* **2001**, *73*, 49−53.
(43) Ma, L.; Feng, S.; de la Fuente-Núñez, C.; Hancock, R. E. W.; Lu, X. Development of Molecularly Imprinted Polymers to Block Quorum Sensing and Inhibit Bacterial Biofilm Formation. *ACS Appl. Mater. Interfaces* **2018**, *10*, 18450−18457.
(44) Cui, Z.; Li, Z.; Jin, Y.; Ren, T.; Chen, J.; Wang, X.; Zhong, K.; Tang, L.; Tang, Y.; Cao, M. Novel magnetic fluorescence probe based on carbon quantum dots-doped molecularly imprinted polymer for AHLs signaling molecules sensing in fish juice and milk. *Food Chem.* **2020**, *328*, No. 127063.
(45) Afsharara, H.; Asadian, E.; Mostafiz, B.; Banan, K.; Bigdeli, S. A.; Hatamabadi, D.; Keshavarz, A.; Hussain, C. M.; Keçili, R.; Ghorbani-Bidkorpeh, F. Molecularly imprinted polymer-modified carbon paste electrodes (MIP-CPE): A review on sensitive electrochemical sensors for pharmaceutical determinations. *TrAC Trends Anal. Chem.* **2023**, *160*, No. 116949.
(46) Frigoli, M.; Lowdon, J. W.; Caldara, M.; Arreguin-Campos, R.; Sewall, J.; Cleij, T. J.; Diliën, H.; Eersels, K.; Van Grinsven, B. Thermal Pyocyanin Sensor Based on Molecularly Imprinted Polymers for the Indirect Detection of Pseudomonas aeruginosa. *ACS Sens.* **2023**, *8*, 353−362.
(47) Hughes, J. P.; Blanco, F. D.; Banks, C. E.; Rowley-Neale, S. J. Mass-producible 2D-WS2 bulk modified screen printed electrodes towards the hydrogen evolution reaction. *RSC Adv.* **2019**, *9*, 25003−25011.
(48) Rowley-Neale, S. J.; Foster, C. W.; Smith, G. C.; Brownson, D. A. C.; Banks, C. E. Mass-producible 2D-MoSe2 bulk modified screen-printed electrodes provide significant electrocatalytic performances towards the hydrogen evolution reaction, Sustain. *Energy Fuels* **2017**, *1*, 74−83.
(49) Whittingham, M. J.; Hurst, N. J.; Crapnell, R. D.; Garcia-Miranda Ferrari, A.; Blanco, E.; Davies, T. J.; Banks, C. E. Electrochemical Improvements Can Be Realized via Shortening the Length of Screen-Printed Electrochemical Platforms. *Anal. Chem.* **2021**, *93*, 16481−16488.
(50) Parsek, M. R.; Greenberg, E. P. Acyl-homoserine lactone quorum sensing in Gram-negative bacteria: A signaling mechanism involved in associations with higher organisms. *Proc. Natl. Acad. Sci. U. S. A.* **2000**, *97*, 8789.
(51) Schooling, S. R.; Charaf, U. K.; Allison, D. G.; Gilbert, P. A role for rhamnolipid in biofilm dispersion. *Biofilms* **2004**, *1*, 91−99.
(52) Morales, D. M.; Risch, M. Seven steps to reliable cyclic voltammetry measurements for the determination of double layer capacitance. *J. Phys. Energy* **2021**, *3*, No. 034013.
(53) Bongaers, E.; Alenus, J.; Horemans, F.; Weustenraed, A.; Lutsen, L.; Vanderzande, D.; Cleij, T. J.; Troost, F. J.; Brummer, R. J.; Wagner, P. A MIP-based biomimetic sensor for the impedimetric detection of histamine in different pH environments. *Phys. Status Solidi* **2010**, *207*, 837−843.
(54) Acet, Ö.; Erdönmez, D.; Acet, B.Ö.; Odabaşı, M. N-acyl homoserine lactone molecules assisted quorum sensing: effects consequences and monitoring of bacteria talking in real life. *Arch. Microbiol.* **2021**, *203*, 3739−3749.
(55) Das, S.; Sarkar, H. S.; Uddin, M. R.; Mandal, S.; Sahoo, P. A chemosensor to recognize N-acyl homoserine lactone in bacterial biofilm. *Sensors Actuators B Chem.* **2018**, *259*, 332−338.
(56) Wang, J.; Quan, C.; Wang, X.; Zhao, P.; Fan, S. Extraction, purification and identification of bacterial signal molecules based on N-acyl homoserine lactones. *Microb. Biotechnol.* **2011**, *4*, 479−490.
(57) Gui, M.; Liu, L.; Wu, R.; Hu, J.; Wang, S.; Li, P. Detection of New Quorum Sensing N-Acyl Homoserine Lactones From Aeromonas veronii. *Front. Microbiol.* **2018**, *9*, 243245.
(58) Hasanah, A. N.; Safitri, N.; Zulfa, A.; Neli, N.; Rahayu, D. Factors Affecting Preparation of Molecularly Imprinted Polymer and Methods on Finding Template-Monomer Interaction as the Key of Selective Properties of the Materials. *Mol.* **2021**, *26*, 5612.
(59) García-Miranda Ferrari, A.; Rowley-Neale, S. J.; Banks, C. E. Screen-printed electrodes: Transitioning the laboratory in-to-the field. *Talanta Open* **2021**, *3*, No. 100032.
(60) Caldara, M.; Lowdon, J. W.; van Wissen, G.; Ferrari, A. G. M.; Crapnell, R. D.; Cleij, T. J.; Diliën, H.; Banks, C. E.; Eersels, K.; van Grinsven, B. Dipstick Sensor Based on Molecularly Imprinted

https://doi.org/10.1021/acsomega.4c03970
ACS Omega 2024, 9, 36411−36420

Polymer-Coated Screen-Printed Electrodes for the Single-Shot Detection of Glucose in Urine Samples—From Fundamental Study toward Point-of-Care Application. *Adv. Mater. Interfaces* **2023**, *10*, 2300182.
(61) Ferrari, A. G. M.; Foster, C. W.; Kelly, P. J.; Brownson, D. A. C.; Banks, C. E. Determination of the Electrochemical Area of Screen-Printed Electrochemical Sensing Platforms. *Biosensors* **2018**, *8*, 53.
(62) Goutelle, S.; Maurin, M.; Rougier, F.; Barbaut, X.; Bourguignon, L.; Ducher, M.; Maire, P. The Hill equation: a review of its capabilities in pharmacological modelling. *Fundam. Clin. Pharmacol.* **2008**, *22*, 633−648.
(63) Guo, L.; Xiao, X.; Chabi, K.; Zhang, Y.; Li, J.; Yao, S.; Yu, X. Occurrence of viable but non-culturable (VBNC) pathogenic bacteria in tap water of public places. *Front. Environ. Sci. Eng.* **2024**, *18*, 1−15.
(64) Wolf-Baca, M.; Siedlecka, A. Community Composition and Antibiotic Resistance of Tap Water Bacteria Retained on Filtration Membranes. *Divers.* **2023**, *15*, 427.
(65) Perera, R.; Ashraf, S.; Mueller, A. The binding of metal ions to molecularly-imprinted polymers. *Water Sci. Technol.* **2017**, *75*, 1643−1650.

https://doi.org/10.1021/acsomega.4c03970
ACS Omega 2024, 9, 36411−36420